On the neural mechanisms of reduced behavior in people with cognitive decline

Tumati, Shankar

CHAPTER 4

Functional network topology associated with apathy in Alzheimer's disease

Submitted as:
Tumati, S., Marsman, J.B.C., De Deyn P.P., Martens S. & Aleman, A., for the Alzheimer's Disease Neuroimaging Initiative
Functional network topology associated with apathy in Alzheimer's disease.

Chapter 4

Abstract

Apathy is a common neuropsychiatric symptom (NPS) in Alzheimer's disease (AD) and is linked to changes in multiple brain regions. However, NPS are often comorbid in AD and functional network changes specific to apathy remain unclear. In AD and mild cognitive impairment patients with low depression scores, topological metrics from resting state functional magnetic resonance images in those with apathy (NPS_A, n=21) were compared to those without NPS (NPS_None, n=28) and those with NPS other than apathy (NPS_NA, n=38). Altered global efficiency, reduced local efficiency and clustering coefficient were found in NPS_A compared to NPS_None and NPS_NA at the whole brain level. In similar contrasts, apathy was associated with increased participation coefficient in the fronto-parietal network and cingulo-opercular network, and reduced local efficiency in the dorsal anterior cingulate network. Apathy in AD is associated with reduced inter-network connectivity of the fronto-parietal network and cingulo-opercular network.

Chapter 4

1. Introduction

Apathy is among the most common neuropsychiatric symptoms (NPS) in Alzheimer's disease (AD) (Geda et al., 2008; Onyike et al., 2007; Spalletta et al., 2010). It is clinically diagnosed by a lack of interest in routine and new activities, and a flat emotional affect (Robert et al., 2009). Symptoms of apathy increase in prevalence and severity as AD progresses from a preclinical stage to mild cognitive impairment (MCI) and later to clinically diagnosed AD (Geda et al., 2008, 2014; Lyketsos et al., 2002). Notably, apathy is associated with a higher risk for disease progression (Palmer et al., 2010), institutionalization and death (Vilalta-Franch, Calvó-Perxas, Garre-Olmo, Turró-Garriga, & López-Pousa, 2013), suggesting that apathy may be a clinical marker for worse pathophysiology in the brain in AD.

Apathy in MCI and AD is associated with changes in brain structure, perfusion, and metabolism (Kos, van Tol, Marsman, Knegtering, & Aleman, 2016; Stella et al., 2014; Theleritis, Politis, Siarkos, & Lyketsos, 2014). The affected regions include the dorsal anterior cingulate cortex, prefrontal cortex, basal ganglia, superior and inferior temporal lobe, and lateral parietal lobe. Though fronto-subcortical disturbances are considered to underlie apathy across disorders (Levy & Dubois, 2006), the involvement of multiple brain regions suggests that diverse neural mechanisms may underlie apathy. Similar investigations of functional mechanisms of apathy that can indicate of the neural circuits involved are few. Moreover, multiple brain regions are known to be impaired progressively in AD (Agosta et al., 2012), but whether these changes contribute to behavioral symptoms is not known.

Resting state functional magnetic resonance imaging (rs-fMRI) has revealed that distant brain regions show correlated activity forming functional networks (Fox & Raichle, 2007). Such networks support specific cognitive functions and changes in these networks are related to neurodegenerative diseases (Seeley, Crawford, Zhou, Miller, & Greicius, 2009). In AD, the default mode network (DMN) shows reduced connectivity and is associated with memory decline and amyloid deposition (Buckner et al., 2005). Two recent studies investigated associations between NPS in AD and functional networks. While Balthazar and colleagues (Balthazar et al., 2014) found no correlations between functional networks and apathy in AD, Munro et al. (Munro et al., 2015) found that the apathy was correlated with reduced connectivity in the fronto-parietal control network (FPCN). However, both studies combined apathy symptoms with other NPS to form a broad category of affective symptoms. As indicated by Munro et al. (Munro et al., 2015), such broader categories may be problematic from a clinical perspective. Moreover, brain changes related to apathy must be separated from comorbid depression, besides other NPS, as apathy and depression are suspected to result from different neural mechanisms (Palmer et al., 2010). In addition, both studies utilized a region-of-interest approach

where a limited number of brain regions are predefined for analysis. Nonetheless, evidence suggests that apathy may be associated with changes in specific functional networks outside the DMN.

Brain networks can be comprehensively characterized by network measures based on graph theory. These metrics describe topological properties of the whole brain as well as of sub-networks (Bullmore & Sporns, 2009). A graph is defined by nodes and their interlinking edges. In rs-fMRI, nodes can be defined as key areas that are denoted as regions of interest (ROI) and the correlation in activation between these ROI defines their edges. Nodes that are connected to each other with a single edge are considered neighbors and the average number of edges between a node and every other node is the path length of that node. The brain is considered to be an optimal network where specialized information can be processed in sub-networks in a segregated manner and processed information can be rapidly integrated globally. These properties of functional segregation and integration can be quantified with measures derived from graph theory (Rubinov & Sporns, 2010). Measures of integration include global efficiency, which is defined as the sum of the inverse of the shortest path length between all pairs of nodes. Measures of segregation quantify the extent of clustering of nodes where specialized information processing can occur. These measures include modularity, clustering coefficient and local efficiency. In large networks, communication is facilitated by nodes that connect to multiple sub-networks. This property is assessed by participation coefficient. All these measures quantify different properties of a network and are further described below.

Studies reporting intrinsic connectivity measures based on graph theory in patients with MCI and AD have reported divergent results regarding both structural and functional brain networks (Brier et al., 2014; Sanz-Arigita et al., 2010; Dai et al., 2015; Tijms et al., 2013; Liu et al., 2014). Relatively consistent findings include increased modularity (Pereira et al., 2016), indicating a loss of functional network organization of the brain, and increased path length that preferentially affects long distance connections (Dai et al., 2015; Deng et al., 2016; Liu et al., 2014). Similar changes have also been reported in the preclinical stage of AD showing changes in modularity and transitivity (similar to clustering coefficient but at network level) from the preclinical stage to mild AD (Brier et al., 2014). Thus, graph measures describe whole brain functional network alterations in AD but no study to our knowledge has investigated such measures in relation to NPS in AD.

Based upon existing literature on apathy and specifically, from empirical associations between brain regions and apathy in AD, we hypothesized that graph theoretical measures of functional sub-networks such as the FPCN and the salience network would be altered in apathy. Further, these localized changes in individual

networks would result in altered graph theoretical measures at the global level. To test this hypotheses, we compared global and network level graph measures in MCI/AD patients with apathy (NPS_A) to those without any NPS (NPS_None), and with those who had NPS other than apathy (NPS_NA). As multiple NPS are often comorbid in MCI/AD, comparison with a NPS_NA group would increase confidence in attributing changes specifically to apathy. Additionally, the AD group was compared with an amyloid negative cognitively normal group to provide a reference with the primary disease process.

2. Methods

Data used in this study were obtained from the Alzheimer's Disease Neuroimaging Initiative (ADNI) database (http://adni.loni.usc.edu). ADNI was launched in 2003 as a public-private partnership, led by Principal Investigator Michael W. Weiner, MD. The primary goal of ADNI has been to test whether serial magnetic resonance imaging (MRI), positron emission tomography (PET), other biological markers, and clinical and neuropsychological assessment can be combined to measure the progression of mild cognitive impairment (MCI) and early Alzheimer's disease (AD). Further information on subject recruitment for this study can be found at http://www.adni-info.org. Written informed consent was obtained from all subjects and study partners. Notably, only those scoring less than 6 on the 15-item Geriatric Depression scale were included.

2.1. Subjects

In the present study, subjects with a baseline rs-fMRI scan from the ADNI2 cohort were included. The analysis consisted of two parts. First, we assessed differences in graph metrics (detailed below) between AD subjects (n=26) and healthy controls (HC, n=18), who were defined as cognitively normal (according to ADNI inclusion criteria) and with cortical amyloid tracer (AV-45) retention below 1.11 standardized uptake value ratio (SUVR) (Landau et al., 2012). This comparison provides a context to changes associated with apathy. Next, three sub-groups were defined within the MCI or AD group - those with i) apathy (AP, n=21), ii) without NPS (NPS_None, n=28), and iii) NPS other than apathy (NPS_NA, n=38). NPS were assessed with the Neuropsychiatric Inventory (NPI, described below).

2.2 Assessments

At baseline, all subjects underwent neuropsychological tests including the Mini Mental State Examination (MMSE), Clinical Dementia Rating (CDR) assessment, and the 13-item Alzheimer's Disease Assessment Scale (ADAS). The NPI is a validated and reliable instrument assessing twelve NPS (Cummings et al., 1994). It is administered to the study partner (known to the subject or preferably living with him/her) in the absence of the

subject and assesses the presence or recent development of NPS in the preceding four weeks. To assess apathy, study partners were asked the following: 'Has the patient lost interest in the world around him/her? Has he/she lost interest in doing things or does he/she lack motivation for starting new activities? Is he/she more difficult to engage in conversation or in doing chores? Is the patient apathetic or indifferent?' Subjects in this study were considered apathetic if the study partner answered 'yes' in response to the above questions. The present study utilized the diagnosis of apathy, and not the severity of apathy symptoms. Other NPS were similarly assessed with symptom-specific questions. The NPS_None group was defined by a total NPI score of zero and the NPS_NA group was defined by a total NPI score greater than zero and NPI-apathy score of zero. In addition to the NPI, the study partner was administered the Functional Assessment Questionnaire (FAQ) (Pfeffer, Kurosaki, Harrah, Chance, & Filos, 1982). All study procedures are described in detail on the study website (http://www.adni-info.org/Scientists/ADNIStudyProcedures.html).

2.3 Image acquisition and processing

An overview of the image processing steps is given in Fig. 1 and described briefly below (Detailed methods in supplementary methods). A seven minute scan was acquired under resting conditions with eyes closed in 3T Philips scanners from 13 sites. The repetition time was 3000ms with a 3.31mm isotropic voxel. A high resolution T1-weighted structural scan was also acquired. Subjects were excluded (n=8) if 40% or more volumes were affected by in-scanner movement (framewise displacement > 0.5mm or intensity variation > 3 standard deviations), resulting in each subject having at least 5 min of minimally affected scans (Power et al., 2014). Further steps included global signal regression, temporal filtering to retain frequencies in the range of 0.009-0.08 Hz, and spatial smoothing with a 6mm full width half maximum kernel. Pearson's correlation coefficient between blood-oxygen level dependent activity in pairs of 264 standard ROI (Power et al., 2011) yielded connectivity matrices, where ROI that were >50% outside scan coverage area in any subject were excluded (28 ROI).

2.4 Network definition

Based on the modularity metric, seven functional networks were defined in the current sample (Fig 2A). These were labeled as - visual network (VS, 52 nodes), somato-motor network (SMN, 43 nodes), insulo-temporoparietal network (Ins-TPN, 39 nodes), FPCN (24 nodes), DMN (64 nodes), dorsal anterior cingulate network (dACC, 6 nodes), and subcortical network (8 nodes). In addition, a standard network definition from independent young healthy subjects was used (Power et al., 2011) (Fig. 2B & supplementary methods). Both network definitions were used as the disease process

may alter healthy network structures but definitions are also influenced by the parcellation method used.

We assessed global efficiency where higher values reflect a more integrated network. Measures of segregation that indicate segregated neural processing were determined at the nodal level with local efficiency and for groups of nodes with clustering coefficient, for both which higher values indicate higher density of edges locally. Segregation was also assessed globally by modularity where higher values indicate increased segregation. For each functional network in both definitions, mean local efficiency representing intra-network density of edges and mean participation coefficient where higher values indicate higher edges within the network or lower inter-network edges (Rubinov & Sporns, 2010). Statistical significance, considered at $p < .05$ (two-sided), for group comparisons adjusted for age and gender was tested non-parametrically using threshold free cluster enhancement (Smith & Nichols, 2009).

3. Results

3.1 Sample characteristics

Table 1 presents demographic, neuropsychological and neuropsychiatric assessments, and imaging characteristics of HC and AD, and MCI and AD subjects with NPS_None, NPS_NA, and NPS_A groups. The NPS_A group showed a worse neuropsychological and AD-related biomarker profile compared to NPS_ None and NPS_NA groups. The NPS_A group had significantly higher CDR scores, reduced functional abilities and a higher total neuropsychiatric burden along with higher cerebral amyloid deposition and lower cerebral glucose metabolism.

3.2 Whole brain topological properties

Graph metrics showed that graph construction methods differentially influence measures. Global efficiency, local efficiency, and clustering coefficient were less stable at network densities below 5%. Modularity reduced with increasing network density in all groups in binary and weighted graphs, whereas global efficiency increased with increasing network density in binary graphs and remained stable in weighted graphs. Local efficiency and clustering coefficient increased with network density in binary graphs but decreased with increasing network density (5-30%) in weighted graphs (Fig. 3).

In the AD group, modularity was significantly higher compared to HC in binary (1-20% network density) and weighted graphs (1-30% network density). No significant differences were found between HC and AD in other global graph metrics. Subjects with apathy showed lower local efficiency compared to NPS_None and NPS_NA groups in binary (8-24% & 9-30% network density, respectively) and weighted graphs (5-30% & 1-

30% network density, respectively). Global efficiency also differed between the groups. However, compared to the NPS_None and NPS_NA groups, global efficiency was lower in the AP group in weighted graphs (10-30% & 9-30% network density, respectively), but higher in binary graphs (5-30% & 2-30% network density, respectively). Clustering coefficient was reduced in the NPS_A group as compared to the NPS_NA group in binary (5-30% network density) and weighted (1-30% network density) graphs. The NPS_A group also showed lower modularity compared to the NPS_NA group but only over a narrow range of network densities in binary graphs (11-13 and 16-22%).

Figure 1: Overview of processing steps

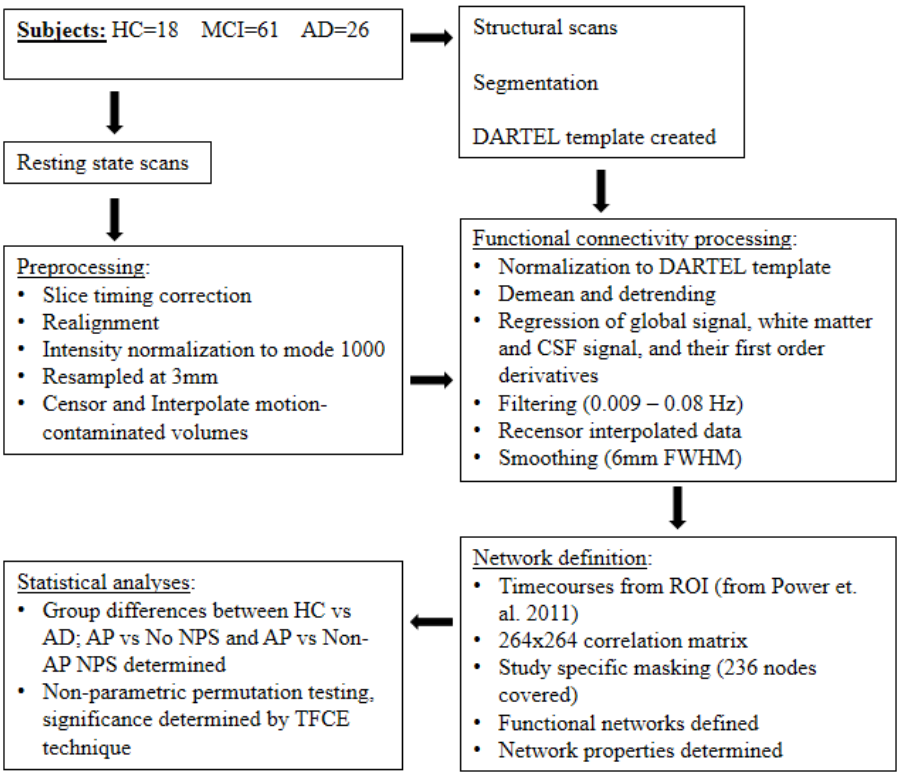

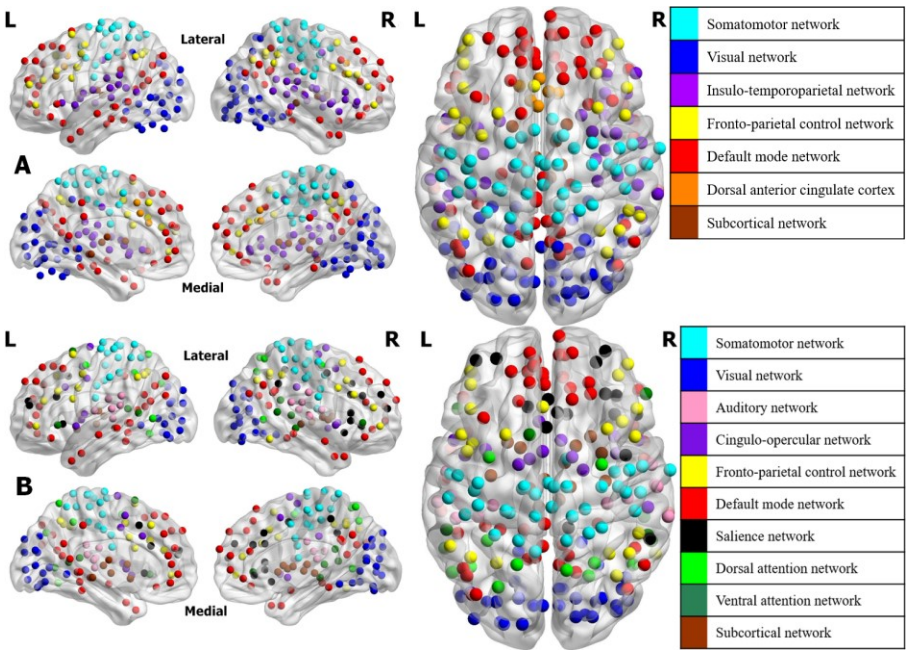

Figure 2: Comparison of functional networks defined in the current study sample (A) and in an independent sample (B) (Power et al., 2011).

The nodes of salience and/pr network in (B) are segregated into a relatively smaller dACC cluster (A) and the insular nodes are coupled with the cingulo-opercular network, which is labelled as the insulo-temporoparietal network in Figure 2A.

3.3 Group differences in functional brain networks

In study-specific networks (Fig. 4), compared to the HC group, the AD group showed significantly reduced local efficiency in the dACC network in binary and weighted graphs (4-28% and 5-30% network density, respectively) and higher participation coefficient in the Ins-TPN (binary: 3-30%, weighted: 4-30%). No further differences were found between HC and AD in other networks. Participation coefficient in the AP group was higher in the FPCN compared to the NPS_NA group (binary: 3-30%, weighted: 3-30%) and lower in the dACC network compared to the NPS_ None group (binary: 8-20, 27-30%, weighted: 8-30%) and the NPS_NA group (binary: 3-30%, weighted: 3-30%). The NPS_None group also showed higher local efficiency in the subcortical network (binary:

3-30%, weighted: 3-30%) and lower participation coefficient in the SMN (binary: 3-30%, weighted: 4-30%) compared to the NPS_A group. Participation coefficient in the subcortical network was lower in the NPS_NA group compared to NPS_A group (binary: 2-24%, weighted: 2-29%).

In network definitions by Power et al. (Power et al., 2011) (Fig. 5), participation coefficient was higher in the VAN in AD compared to HC (binary: 4-30%, weighted: 7-30%). No other significant differences were found between HC and AD in any network. Compared to the NPS_None and NPS_NA group, the NPS_A group showed higher participation coefficient in the FPCN (binary: 5-30%, weighted: 5-30% & binary: 2-30%, weighted: 2-30%, respectively), CON (binary: 5-30%, weighted: 6-30% & binary: 7-30%, weighted: 7-30%, respectively), and SAN (binary: 8-30%, weighted: 8-30% & binary: 13-17, 19-20%, weighted: 13-16, 19%, respectively). The NPS_A group showed higher local efficiency than the NPS_NA group in the DAN (binary: 1-30%, weighted: 1-30%).

Table 1: Sample characteristics of healthy control and AD, and MCI and AD subjects without any NPS (NPS_None), with NPS other than apathy (NPS_NA), and apathy (NPS_A)

	HC	AD	No NPS	Non-AP NPS	AP	Chi-sq$^{\$}$	*p*
n (female)	18 (11)	26 (12)	28 (12)	38 (21)	21 (5)	5.39	.07
n (AD)	-	-	4	12	10	6.38	.04
Age	73.13 (5.7)	72.87 (7.2)	71.22 (6.3)	71.29 (7.6)	75.27 (5.7)	5.18	.07
Education	16.56 (1.8)	15.88 (2.7)	16.18 (2.5)	16.16 (2.7)	15.76 (2.6)	0.41	.81
MMSE	28.61 (1.5)	22.35 (2.5)	26.75 (3.0)	26.05 (3.2)	25.48 (3.4)	2.38	.30
ADAS-13	9.28 (3.9)	35.58 (9.2)	19.71 (11.4)	20.08 (11.4)	25.57 (12.5)	4.01	.13
CDR-SB	0.03 (0.1)	4.40 (1.4)	1.64 (1.5)	2.49 (1.6)	3.57 (1.6)	18.62	<.01

FAQ	0.11 (0.5)	15.00 (7.8)	3.70 (6.9)	7.26 (7.9)	12.19 (6.0)	22.12	<.01
Total NPI	0.61 (1.0)	9.23 (11.3)	-	5.13 (5.2)	12.81 (11.1)	10.76	<.01[#]
Hippocampal volume (bilateral, mm^3)	7029.2 (783.8)	6068.7 (1050.0) (n=23)	7085.7 (1070.6) (n=23)	6837.20 (1369.6) (n=36)	6637.41 (933.0) (n=19)	1.05	.59
Amyloid uptake (AV45)	1.02 (0.04)	1.47 (0.2) (n=25)	1.22 (0.2)	1.31 (0.2) (n=37)	1.39 (0.3)	6.21	.04
FDG-PET	6.79 (0.4)	5.24 (0.7)	6.17 (0.9)	6.02 (0.7)	5.64 (0.6)	8.37	.02

[$] Chi-square statistic for Kruskal-Wallis test (two-tailed); [#] comparison between No-AP NPS and AP groups; AV45: Amyloid binding ligand, values in Standardized Uptake Value Ratio (SUVR); FDG-PET: Glucose metabolism, values in SUVR; ADAS-13: Alzheimer's Disease Assessment Scale-13 item; FAQ: Functional Assessment Questionnaire; CDR-SB: Clinical Dementia Rating scale-sum of boxes; NPI: Neuropsychiatric Inventory score

Further, the NPS_None group showed higher local efficiency in the subcortical network (binary: 20-27%, weighted: 16-30%) and lower participation coefficient in the SMN (binary: 3-30%, weighted: 3-30%) than in the NPS_A group. Finally, the NPS_NA group showed higher local efficiency (binary: 11-25%, weighted: 4-30%) and lower participation coefficient (binary: 8-10%, weighted: 6-29%) in the DMN as compared to the NPS_A group.

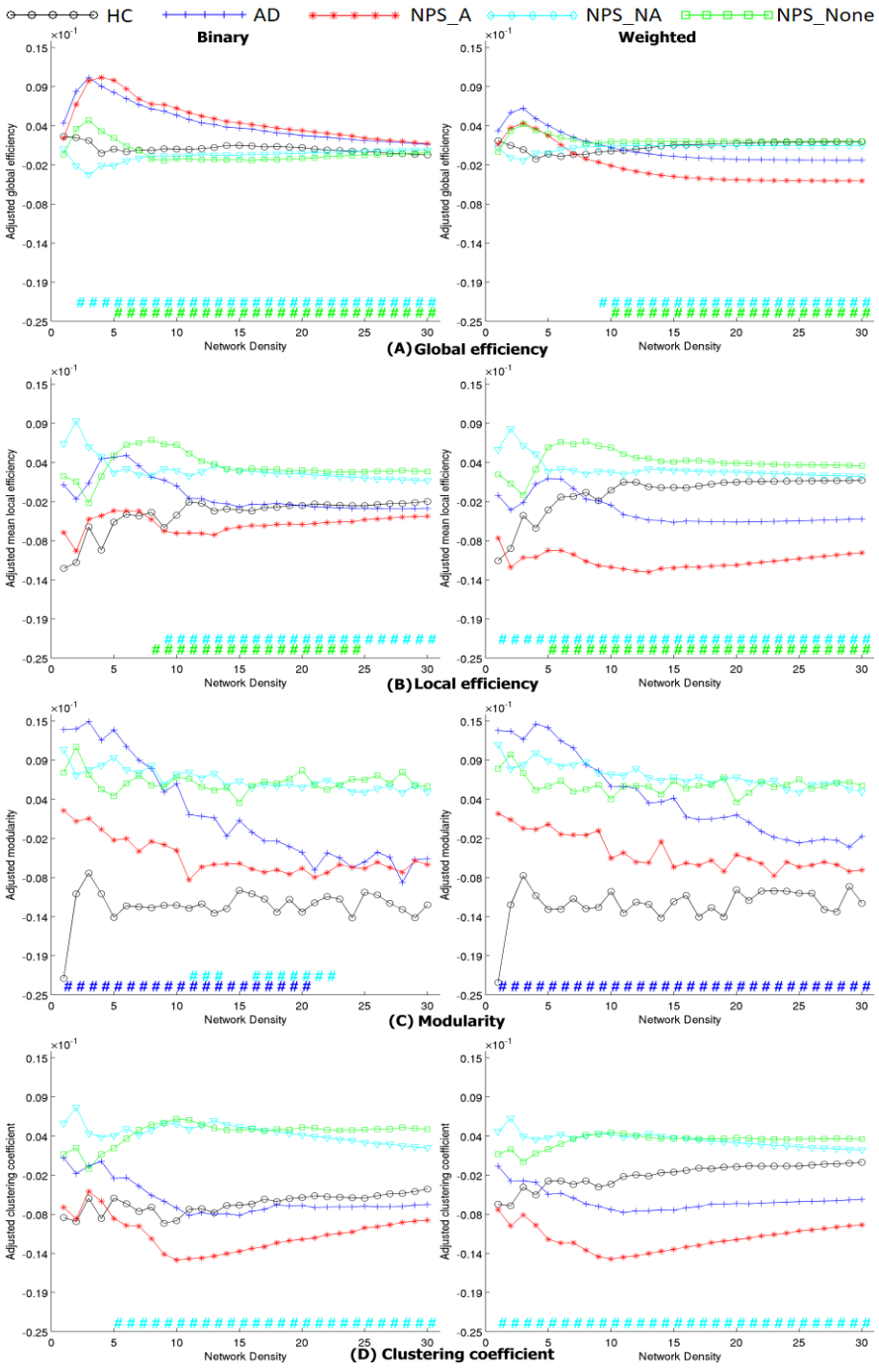
HC
AD
NPS_A
NPS_NA
NPS_None
Binary
Weighted
Adjusted global efficiency
Network Density
(A) Global efficiency
Adjusted mean local efficiency
(B) Local efficiency
Adjusted modularity
(C) Modularity
Adjusted clustering coefficient
(D) Clustering coefficient

Figure 3: Whole brain graph theoretical measures (previous page)

The figures show the binary (left) and weighted (right) global efficiency (A), mean local efficiency (B), modularity (C) and clustering coefficient (D) (y-axis) over increasing network densities (x-axis), after adjustment for age and gender, for each group. Each hash (#) symbol (aligned to the x-axis) indicates a significant difference at each network density with the color indicating the groups compared. Dark blue (**#**) indicates significance for HC vs AD. Light blue (#) indicates significance for NPS_NA vs NPS_A. Light green (#) indicates significance for NPS_None vs NPS_A. In those with AD compared to HC, modularity was higher (C) suggesting increased segregation of networks. In NPS_A, local density of connections are lower as suggested by lower local efficiency (B) and clustering coefficient (D) whereas global efficiency in the AD and NPS_A groups are highly similar (A).

Figure 4: Graph theoretical properties in current sample networks (next page)

The figures show the binary (left) and weighted (right) mean local efficiency (y-axis) in the dACC (A), and mean participation coefficient (y-axis) over increasing network densities (x-axis) in the dACC (B), Insulo-temporoparietal network (C), and frontoparietal control network (D), after adjustment for age and gender, for each group. Each hash (#) symbol (aligned to the x-axis) indicates a significant difference at each network density with the color indicating the groups compared. Dark blue (#) indicates significance for HC vs AD. Light blue (#) indicates significance for NPS_NA vs NPS_A. Light green (#) indicates significance for NPS_None vs NPS_A. The NPS_A group shows similar changes as the AD group in local efficiency in dACC (A) and participation coefficient in the insulo-temporoparietal network (C). However, participation coefficient of the dACC (B) in the NPS_A group and AD diverge. Taking (A) and (B) together suggests that inter-network edges in NPS_A are lost to a greater extent than in AD. In contrast, changes in FPCN in form of increased participation coefficient may be specific to the NPS_A group.

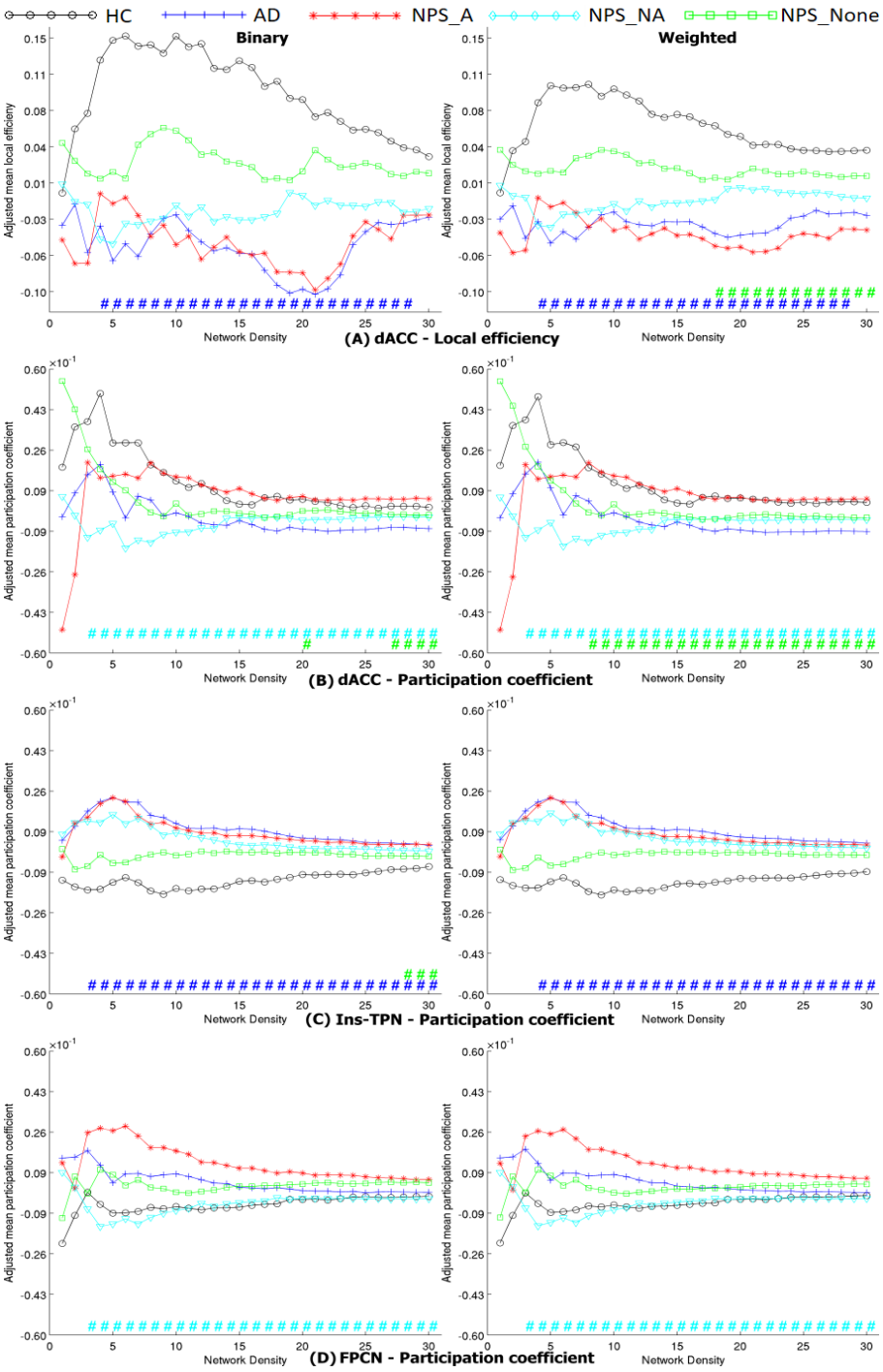
HC
AD
NPS_A
NPS_NA
NPS_None
Binary
Weighted
Adjusted mean local efficiency
Network Density
(A) dACC - Local efficiency
Adjusted mean participation coefficient
(B) dACC - Participation coefficient
(C) Ins-TPN - Participation coefficient
(D) FPCN - Participation coefficient

4. Discussion

This study aimed to determine topological properties of functional brain networks associated with apathy in MCI and AD. Subjects with apathy were more likely to have AD, have higher scores on the CDR-SB, NPI and FAQ, and higher global amyloid deposition, and lower cortical glucose metabolism compared to those without any NPS and those with NPS other than apathy. In topological measures, the AD group showed increased modularity while global efficiency, local efficiency and clustering coefficient were similar as compared to the HC group. In contrast, those with apathy showed lower local efficiency and clustering coefficient, suggesting that segregated neural processing is affected. Global efficiency was also altered in the NPS_A group, whose values were highly similar to the AD group (Fig 3). These results suggest that apathy may be associated with reduced nodal density of functional connections. The findings from network level analysis in both network definitions converge upon the FPCN where participation coefficient was higher while local efficiency was similar in NPS_A compared to the NPS_None and NPS_NA groups. This suggests that lower inter-network connectivity of the FPCN is associated with apathy in AD. Similarly, inter-network connectivity in the CON is lower in NPS_A than in NPS_NA and NPS_None. In addition, the dACC showed lower local efficiency than in NPS_NA and NPS_None suggesting that reduced intra-network connectivity in the dACC may play a role in producing symptoms of apathy.

Symptoms of apathy have been proposed to arise from deficits in neural circuits linking the frontal cortex to the basal ganglia (Levy & Dubois, 2006). As noted above, apathy in MCI and AD patients is associated with only the frontal-subcortical circuits but with broader regions of the association cortex and particularly with regions that support goal-directed actions (Kos et al., 2016; Stella et al., 2014; Theleritis et al., 2014). The findings of this study show that functional connectivity between the FPCN and CON to other networks is reduced in apathy. These networks support control of goal-directed action by dynamically regulating executive functions in the FPCN, and the maintenance of sustained attention and task-representations in the CON (Dosenbach et al., 2007; Sadaghiani et al., 2010; Seeley et al., 2007). That changes in both networks indicate reduced inter-network connectivity suggests that patients with apathy experience difficulties in transforming goal representations to goal-directed actions but not in the neural processing of each set of functions independently. This interpretation is consistent with apathy symptoms such as an inability to initiate actions but once initiated, capacity to execute the action is preserved.

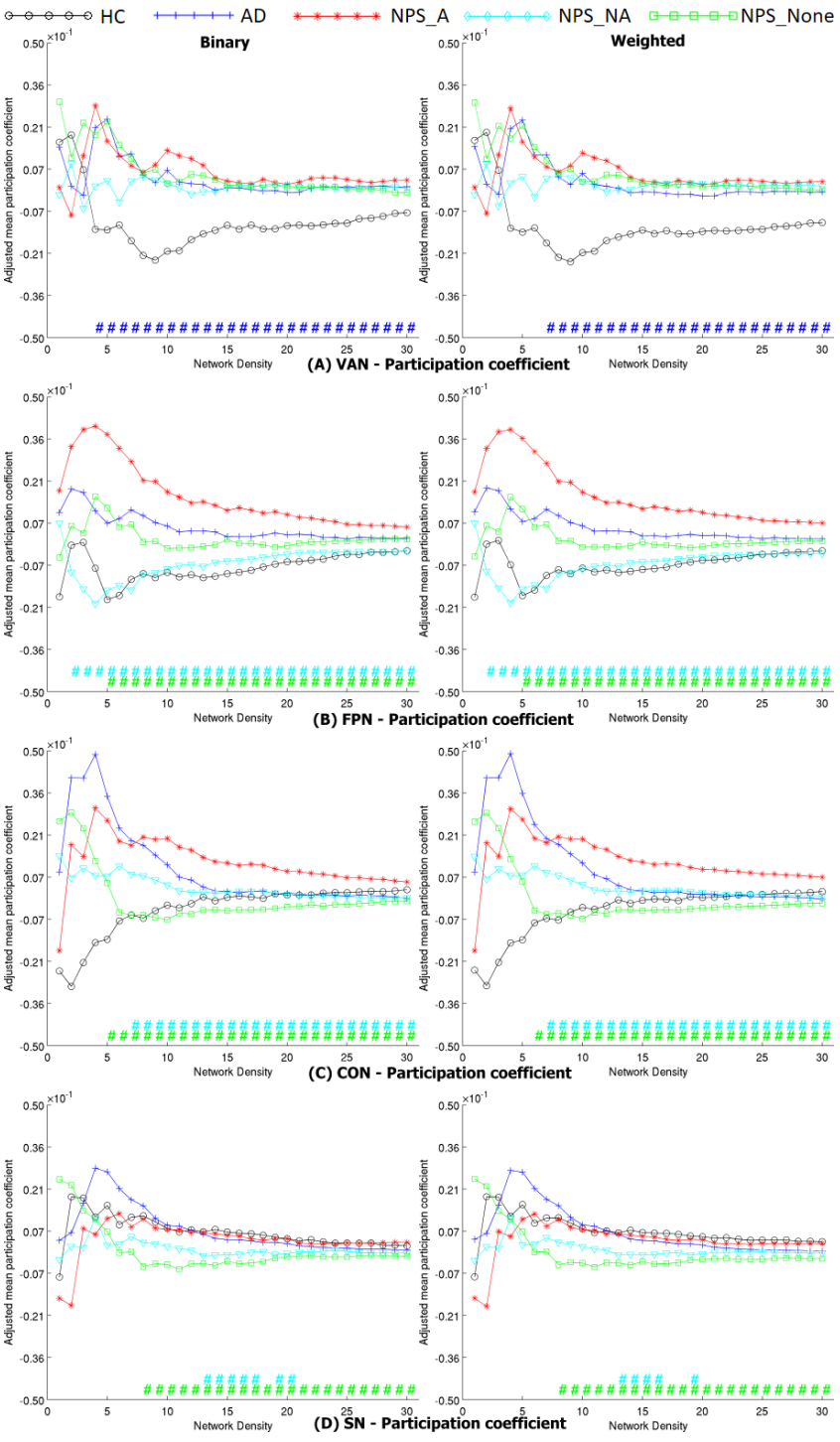
HC
AD
NPS_A
NPS_NA
NPS_None
Binary
Weighted
Adjusted mean participation coefficient
Network Density
(A) VAN - Participation coefficient
(B) FPN - Participation coefficient
(C) CON - Participation coefficient
(D) SN - Participation coefficient

Figure 5: Group difference in independently-defined networks (previous page)
The figures show the binary (left) and weighted (right) mean participation coefficient (y-axis) over increasing network densities (x-axis) in the ventral attention network (A), frontoparietal control network (B), cingulo-opercular network (C), and salience network (D), after adjustment for age and gender, for each group. Each hash (#) symbol (aligned to the x-axis) indicates a significant difference at each network density with the color indicating the groups compared. Dark blue (**#**) indicates significance for HC vs AD. Light blue (#) indicates significance for NPS_NA vs NPS_A. Light green (#) indicates significance for NPS_None vs NPS_A. Increased participation coefficient in the frontoparietal control network (B) and cingulo-opercular network (C) was present to a greater extent in the NPS_A group whereas all patient groups show similarly increased participation coefficient in the ventral attention network (A). In the salience network (D), the NPS_None group shows lower participation coefficient, which may indicate compensatory changes that preserve function.

It may also be that both networks communicate independently with other networks controlling the generation of behavior that may be deficient. This interpretation would suggest that the neural routes to the development of apathy may differ between patients with apathy.

This study expands upon previous results that associated apathy in MCI/AD to broad brain regions and particularly to the dACC and temporo-parietal lobe (Stella et al., 2014; Theleritis et al., 2014). A recent functional connectivity study found that apathy was associated with reduced connectivity in the FPCN in association with apathy in MCI patients (Munro et al., 2015). ROI were limited to four functional networks and inter-network connectivity was not investigated. As NPS increase in number and severity with stages of AD, they are often comorbid and associating brain changes to specific NPS is not trivial. In the current study, a novel approach was used contrasting apathy with those without NPS and those with NPS_NA. When differences are present in both comparisons, the findings are more likely to be specific to apathy. Moreover, the parent ADNI study excluded subjects with high depression scores at baseline, which reduces the likelihood of overlapping symptomatology and confounding neural changes. Finally, this study investigated network topology in the whole brain that enabled detection of intra- and inter-network connectivity changes in fine-grained brain networks. Thus, the results from the current study may be considered to reflect brain changes underlying apathy more accurately as compared to past studies.

In the broader context of graph theoretical changes seen in AD, the apathy sub-group showed similar changes to the complete AD group in global efficiency but modularity in apathy is altered to a smaller degree (Fig. 3). Local efficiency and clustering coefficient were altered to a greater extent in the apathy group than in complete AD group. In AD, long distance connections are posited to be more affected than short distance connections (Dai et al., 2015; Deng et al., 2016; Liu et al., 2014). Taken together, it may be that loss of functional connectivity at a nodal level plays a large role in the producing symptoms of apathy. Considering that the apathy group comprised of MCI and AD patients, the larger differences in this group compared to the AD group may also underlie the increased risk for disease progression seen in those with apathy in AD. Furthermore, the pattern of changes in individual networks seen in Fig. 3 & 4 suggests that NPS can reveal localized network changes in AD. For example, participation coefficient was similar in all patient groups in the ventral attention network (Fig. 3) but lower in the somatomotor network of the NPS_None group (Supplementary figures). Thus, NPS may reveal localized network changes and their role in the general network dysfunction in AD need to be further investigated.

4.1 Limitations

Graph theoretical measures are sensitive to methodological procedures, which have been suggested to result in differences between studies (Tijms et al., 2013). In this study for example, AP was associated with higher GE in binary graphs but reduced GE in weighted graphs. Such results highlight the complexity of graph measures and interpreting such findings may be challenging (De Vico Fallani, Richiardi, Chavez, & Achard, 2014). Processing steps such as ignoring negative correlations in building graphs or the use of global signal regression may also affect results. Therefore, replication of findings in an independent sample is essential. Furthermore, the organization of brain networks is affected by variables such as age and disease. By using functional networks defined in a healthy independent sample and in the study sample, we aimed to minimize such effects. Nevertheless, methodological differences in defining the network structures need to be considered. Finally, using the NPI to diagnose apathy can be considered a limitation as studies indicate that apathy is a complex construct that can be separated into sub-types that may have distinct neural mechanisms (Levy & Dubois, 2006). Future studies may investigate if there are multiple routes to apathy in AD.

In summary, the results of the current study in a sample with low depression scores suggest that reduced inter-network connectivity of the frontoparietal control network and the cingulo-opercular network is associated with apathy in AD. Further, the dACC shows a marked reduction in efficiency and segregation in association with apathy. Finally, global changes suggest that apathy is specifically associated with localized loss of functional connections.

Supplementary Information

Supplementary Methods

Image acquisition: Subjects were scanned on 3.0 Tesla Philips MRI scanners at thirteen sites. Echoplanar images with repetition time/echo time (TR/TE) of 3000/30 ms and flip angle (FA) of 80° were acquired in an interleaved manner. Each scan consisted of 140 volumes, with 48 slices, dimensions 64 x 64 and voxel size 3.31 x 3.31 x 3.31 mm. Structural images with a resolution of 1 x 1 x 1.2 mm were acquired through the sagittal plane, using a magnetization prepared rapid gradient echo (MPRAGE) three-dimensional T1-weighted sequence with a TR = 6.8 ms, TE = 3.16 ms, and FA = 9°. Scans were acquired a maximum of 81 days prior to NPI assessment (mean (SD) = 18.6 (15.0) days).

Image pre-processing: An overview of the methods are provided in Fig. 1. rs-fMRI data were preprocessed with the following steps: i) first three volumes of the resting state scans were discarded to achieve signal equilibrium; ii) scans were corrected for slice timing and intensity differences due to interleaved acquisition; iii) scans were spatially realigned to the first volume using rigid body transformation to correct for head motion within runs, and then coregistered to the subject's high resolution structural scan; iv) scans were intensity scaled within runs to a mode value of 1000 (performed using *fslmath* in the FSL suite), and v) normalized to a study specific anatomical template created using DARTEL (Diffeomorphic Anatomical Registration through Exponentiated Lie Algebra toolbox) and resampled to 3mm isotropic voxels. To minimize motion-induced spurious correlations (van Dijk, Sabuncu and Buckner, 2012; Power et al., 2014), scans were examined for excessive motion defined by framewise displacement (FD) and standardized delta variations in signal intensity (DVARS). FD estimates head motion from one volume to next and is calculated as the sum of the absolute displacement in translational and rotational motion. Rotational measures were transformed to millimeters by assuming that the center of rotation was located 65mm away from the affected voxels. The DVARS measure determines changes in signal intensity from one volume to the next and is calculated at the global level as the root mean square of the temporal derivative of the time series at each voxel. Volumes where FD exceeded 0.5mm and DVARS exceeded 3 standard deviations (with first volume set at zero) were censored. If less than five minutes of valid volumes (100 volumes, 73% of the scan) remained after censoring then scans were excluded from further analysis (n=8). For remaining scans, censored volumes were replaced by spline interpolation, and were re-censored after frequency filtering. On average, 5.08 % volumes in each scan were censored (AD=4.2%, MCI=4.29%, SMC=5.7%, HC=6.9%). To further reduce spurious effects, additional steps were performed including demeaning and linear detrending the signal, regressing out 1) the global signal, 2) white matter, 3) cerebrospinal fluid signal and 4) motion parameters from the realignment step, and their first order derivatives.

We chose to perform global signal regression as it was shown to strongly reduce motion related artifacts when combined with censoring of motion affected volumes and reduces the need to censor volumes subsequent to the movement affected volume (Power et al., 2014). Next, temporal band pass filtering using an eighth order Butterworth filter with zero phase was performed to retain frequencies in the range of 0.009 to 0.08 Hz. Finally, data were spatially smoothed with a 6mm FWHM (full width half maximum) kernel.

Connectivity matrices: To determine functional connectivity, first subject specific masks were created by binarizing the processed scans using BET tool in the FSL suite. Regions of interest (ROI) with less than 50% coverage in any subject were excluded for all subjects (28 ROI). The mean time-course from each remaining ROI was extracted and Pearson's correlation coefficient between each pair of ROI was calculated, generating a 236 x 236 matrix for each subject. For ROI at a distance of less than 20mm apart, the correlations were set to zero as such correlations may result from motion induced artifacts and/or smoothing process. Further, correlations between a ROI and itself were set to zero. Negative correlations were also set to zero as negative correlations can be introduced spuriously when global signal regression is performed (Murphy et al., 2009; Weissenbacher et al., 2009), which lead to reduced test-retest reliability (Shehzad et al., 2009; Wang et al., 2011). The final outcome matrix, referred to as the connectivity matrix hereafter, was used in all subsequent steps.

Network definition: The nodes of a graph can be separated into non-overlapping communities or modules by maximizing the modularity metric, which quantifies the extent to which a module has maximum within-module edges and minimum between-module edges. The resulting modules are labeled functional networks. However, such definitions are subject to methodological choices and may differ between study populations. Therefore, we defined functional networks based on the current study sample. The modularity metric was determined at a single optimal threshold, which was determined by computing entropy values obtained by applying information theory to the connectivity matrices (See Geerligs et al., 2015 for details of this method). Briefly, connectivity matrices were thresholded proportionally over a range of values (1-50%) in incremental steps of 1%, where the threshold proportion of strongest correlations in the matrix at each step were retained such that the matrix is converted to represent the retained correlation values as present and the rest as absent. The binarized matrices were then averaged over subjects and entropy values were calculated. These steps were performed separately for the HC, MCI, and AD groups to allow for variations in the optimal threshold according to group. As entropy values are sensitive to the number of edges, which differ according to the applied threshold, random matrices with the same number of edges at each threshold were created for comparison. The following process

was used to generate the random matrices - 50 randomized matrices with the same number of nodes and edges were generated at each threshold per subject. From these random matrices, 500 new average matrices were created per group by sampling the randomized matrices at each threshold. The random matrices per group were then averaged and entropy values were calculated at each threshold. Finally, entropy values of the random matrices and true matrices were compared. The threshold at which the lowest entropy in the true matrices across groups maximally differed from the lowest entropy of the randomized matrices was determined as the optimal threshold. For all groups, the optimal threshold value was determined at a threshold value of 1%.

The optimal threshold was used to partition the connectivity matrices into non-overlapping modules (Newman, 2004). In order to obtain smaller modules, the modularity metric used for partitioning was maximized across a range of resolutions. First, an initial partition was created for each connectivity matrix using the Louvain modularity algorithm (Blondel, Guillaume, Lambiotte and Lefebvre, 2008). Next, a fine-tuning algorithm was applied to increase modularity, and a new partition was obtained (Sun, Danila, Josić and Bassler, 2009). This process was repeated 50 times and each node was assigned to a module. The node assignments over the 50 repetitions were then averaged to create a single consensus matrix per subject. The consensus matrix per subject was then re-entered into the above steps to obtain new partitions. This step was repeated until the consensus matrix per subject remained unchanged and was considered stable.

To achieve stable partitioning across subjects, consensus matrices of all subjects were averaged and entered into a consensus partitioning algorithm (Lancichinetti and Fortunato, 2012) at 30 resolutions (ranging 1 to 3, in steps of 0.1). The resulting group consensus matrices at each resolution were assessed for similarity across the resolutions. This was achieved by comparing the normalized mutual information (NMI) across each resolution. Across all resolutions, a 7-module decomposition was found most often (13 times), which showed a mean NMI of 0.93. Identical partitioning (NMI=1) was present at four resolutions and was used to define functional networks in subsequent analyses (Fig. 2A). We then repeated the analyses using a network definition based on an independent sample of healthy young adults (Power et al., 2011) (http://www.nil.wustl.edu/labs/petersen/Resources.html) to provide comparability with previous studies. In this network definition, nodes with inadequate coverage, those defined as uncertain (11 nodes), as part of cerebellar network (4 nodes), and a posited memory retrieval network (5 nodes) were excluded. Nodes classified separately as sensory-motor hand (29 nodes) and sensory-motor mouth (5 nodes) networks were combined. These steps resulted in a total of 10 functional networks (216 nodes) (Fig. 2B).

Network Measures: Connectivity matrices were thresholded over a range (1-30%), retaining the proportionate number of strongest correlations. Thresholding over a range of edge strengths is required, as including all edges results in a fully connected graph, while using a single threshold uses an arbitrary set of functional connections. Binary and weighted thresholded matrices were used to calculate network measures. Both types of measures were determined because binarizing matrices may introduce bias as correlations close to the threshold value are similar but may be included or excluded, resulting in artificial variations in edges between subjects [6]. Using weighted graphs reduces this bias and enhances reproducibility but methods for scaling edge weights are currently not definitive.

The following network measures were determined using the Brain Connectivity Toolbox (Rubinov and Sporns, 2010). Three measures were calculated using whole brain graphs - global efficiency, local efficiency, and modularity. Global efficiency is the sum of the inverse of the average path between all pairs of nodes in a graph with higher values indicating more efficient paths between each node to any other node in the network. Local efficiency is calculated as the inverse of the average path length between a node and its immediate neighbors. Higher local efficiency indicates higher density of edges locally. For the whole brain graph, local efficiency of each node is averaged. Modularity quantifies the extent of segregation of nodes in a graph into modules or networks. Segregation of networks allows each network to process specialized information. Higher modularity values indicate better segregation between networks. Further, for each functional network, local efficiency and participation coefficient were calculated. In this case, local efficiency of each node and the mean value for a network were restricted to edges within the network. Participation coefficient determines the ratio of intra-network edges to all edges of a node and the mean of these values from each node within a network indicated the extent of intra- or inter-network edges. Higher values indicate better integration between networks.

Statistical analysis: Differences in graph measures between i) HC and AD, ii) NPS_None and NPS_A, and iii) NPS_NA and NPS_A were determined after controlling for age and gender. Significance of the differences in network measures was non-parametrically tested by randomly permuting group membership 5000 times for each comparison (maintaining group sizes). A null distribution of group differences for each comparison was computed at each threshold and tested for significance using threshold free cluster enhancement (TFCE) (with default settings-E=0, H=1) (Smith and Nichols, 2009). Results were considered significant at a two-sided p value of < .05. All analyses were conducted in MATLAB 2014a (The MathWorks, Inc., Natick, USA), unless noted otherwise, using custom in-house scripts. Preprocessing steps (except intensity normalization) were

performed in SPM12b (http://www.fil.ion.ucl.ac.uk/spm/software/spm12). Fig. 2 was created using BrainNet Viewer (http://www.nitrc.org/projects/bnv/).

Supplementary Figures A-E: Group difference in current-sample and independently-defined networks

The figures show the binary (left) and weighted (right) mean participation coefficient (y-axis) over increasing network densities (x-axis). Fig A shows local efficiency and Fig B shows participation coefficient in networks defined in the current sample. Fig C and D show local efficiency and Fig E shows participation coefficient in networks defined in an independent sample. Measures in all figures are adjusted for age and gender. Each hash (#) symbol (aligned to the x-axis) indicates a significant difference at each network density with the color indicating the groups compared. Dark blue (**#**) indicates significance for HC vs AD. Light blue (#) indicates significance for NPS_NA vs NPS_A. Light green (#) indicates significance for NPS_None vs NPS_A.

DMN: Default mode network; DAN: Dorsal attention network; VAN: ventral attention network; FPN: frontoparietal network, CON: cingulo-opercular network, SN: salience network; Ins-TPN: insulo-temporoparietal network; AN: auditory network; VN: Visual network; SMN: somatomotor network;

SI Figure A

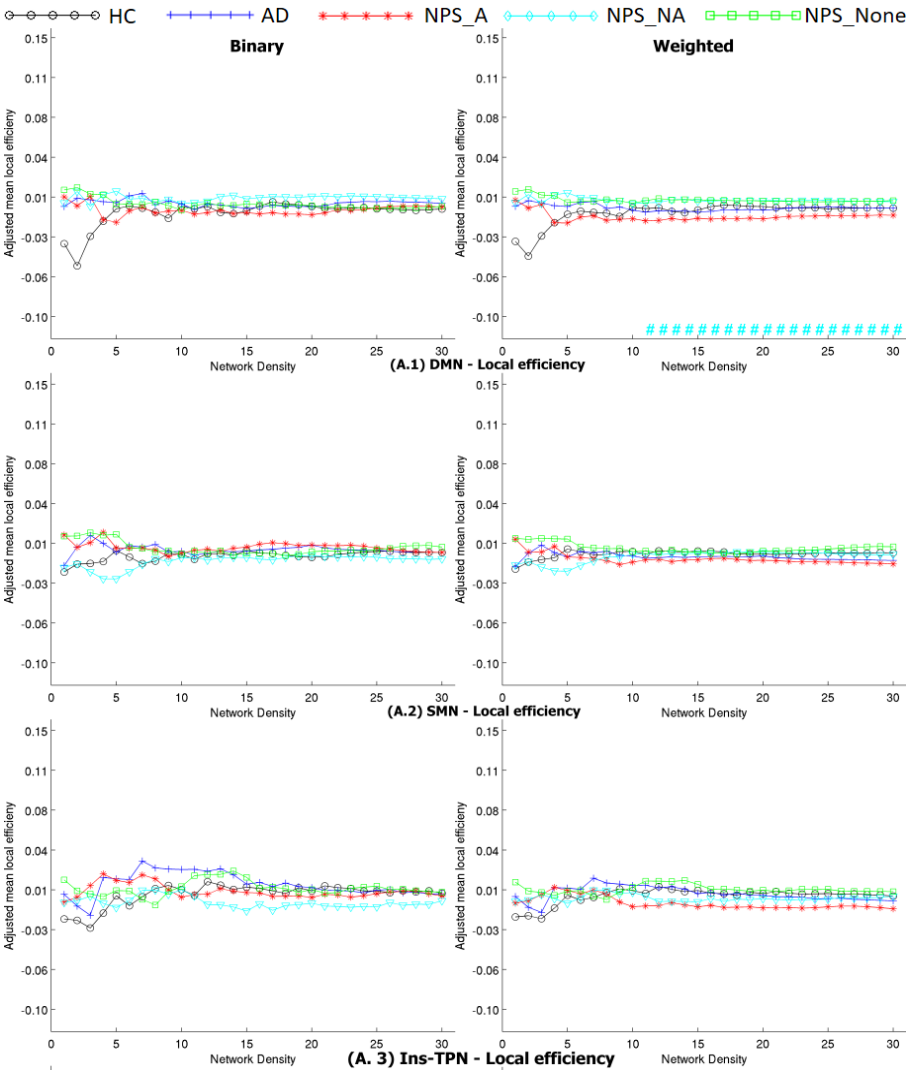
HC
AD
NPS_A
NPS_NA
NPS_None
Binary
Weighted
Adjusted mean local efficieny
Network Density
(A.1) DMN - Local efficiency
(A.2) SMN - Local efficiency
(A. 3) Ins-TPN - Local efficiency

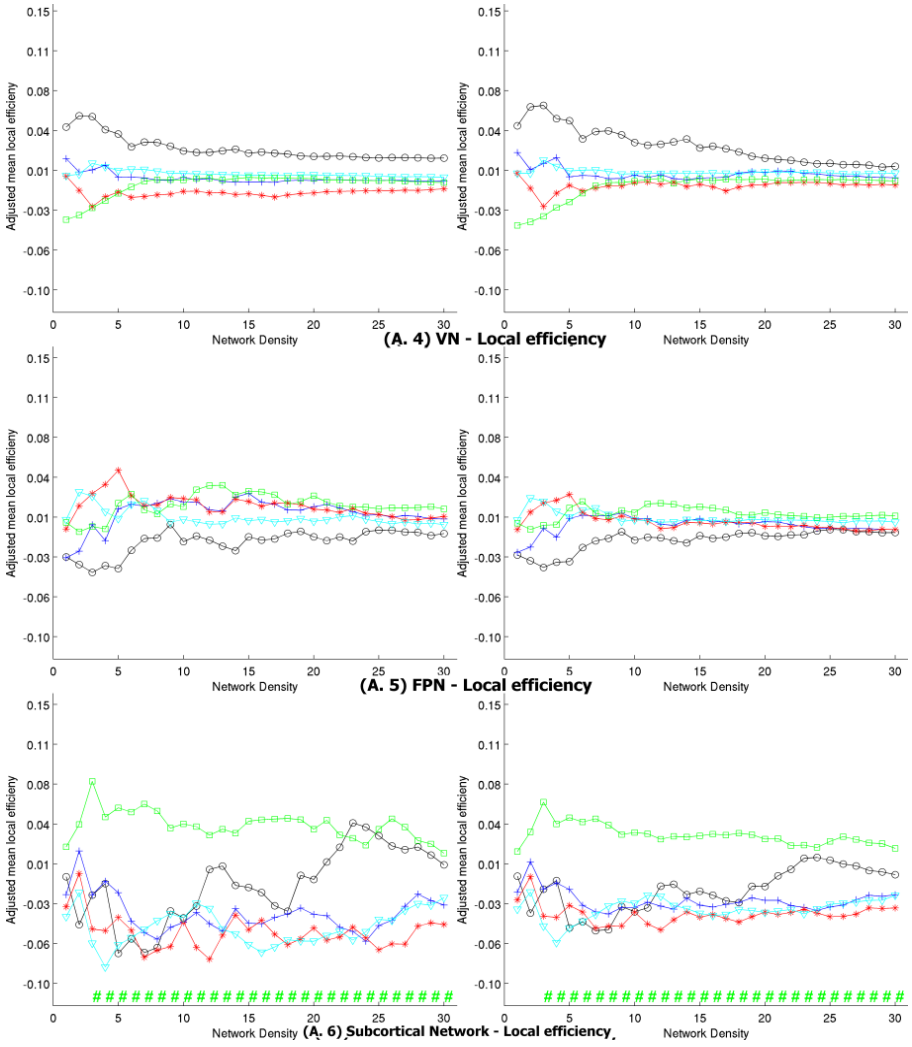
Adjusted mean local efficiency
Network Density
(A. 4) VN - Local efficiency
(A. 5) FPN - Local efficiency
(A. 6) Subcortical Network - Local efficiency

SI Figure B

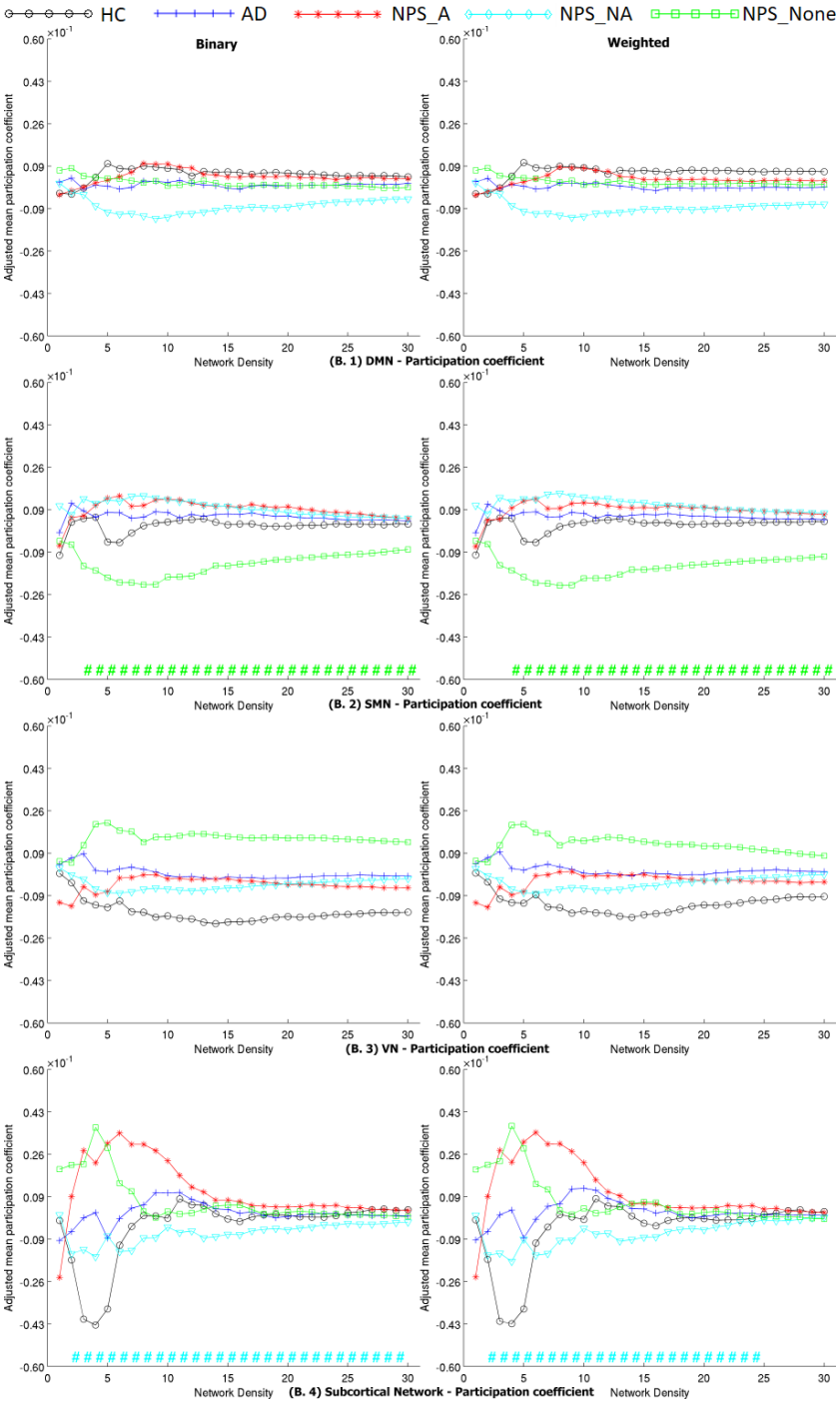
HC
AD
NPS_A
NPS_NA
NPS_None
Binary
Weighted
Adjusted mean participation coefficient
Network Density
(B. 1) DMN - Participation coefficient
(B. 2) SMN - Participation coefficient
(B. 3) VN - Participation coefficient
(B. 4) Subcortical Network - Participation coefficient

SI Figure C

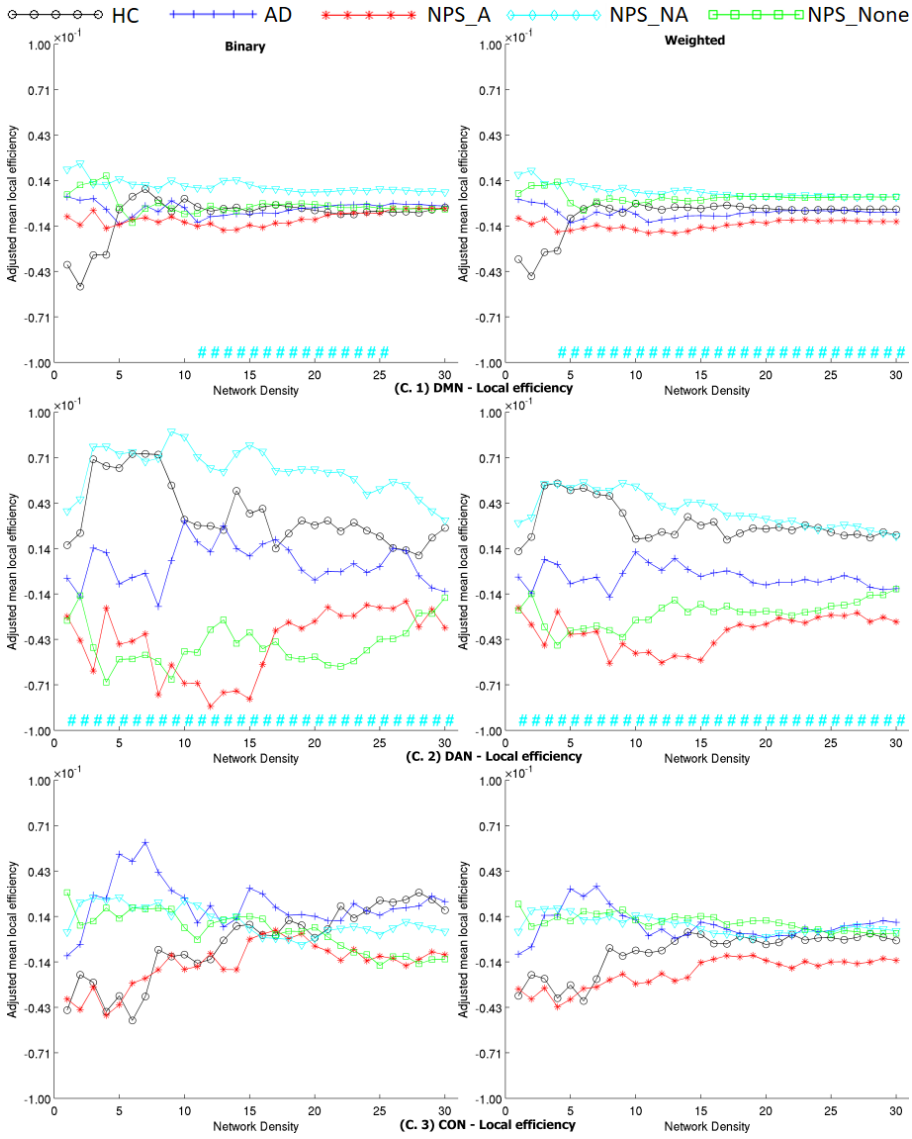
HC
AD
NPS_A
NPS_NA
NPS_None
Binary
Weighted
Adjusted mean local efficiency
Network Density
(C. 1) DMN - Local efficiency
(C. 2) DAN - Local efficiency
(C. 3) CON - Local efficiency

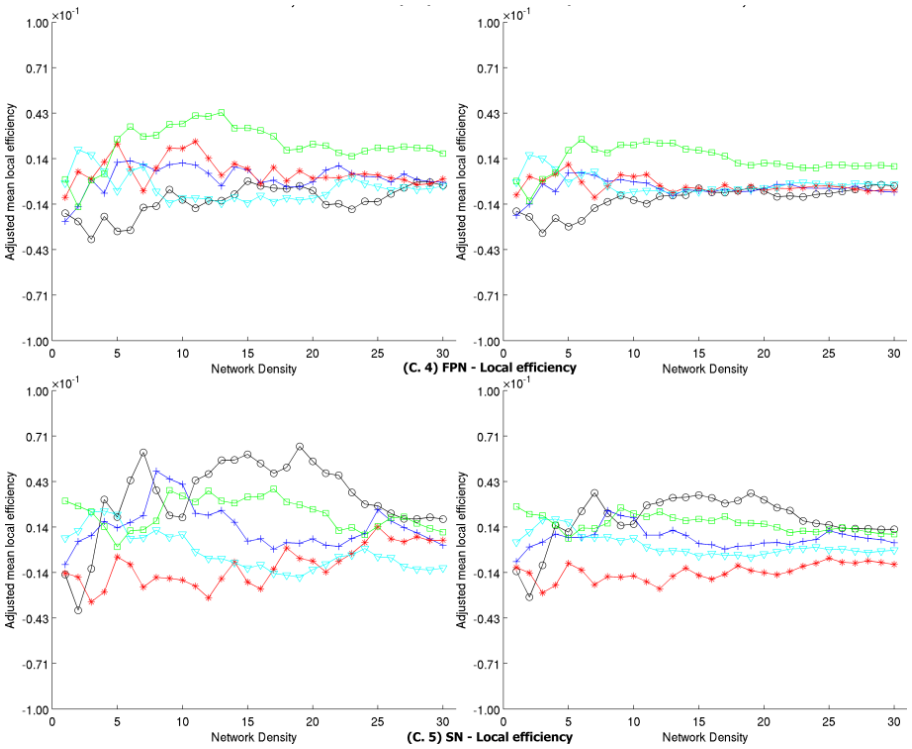
×10^-1
1.00
0.71
0.43
0.14
-0.14
-0.43
-0.71
-1.00
Adjusted mean local efficiency
0
5
10
15
20
25
30
Network Density
(C. 4) FPN - Local efficiency
(C. 5) SN - Local efficiency

SI Figure D

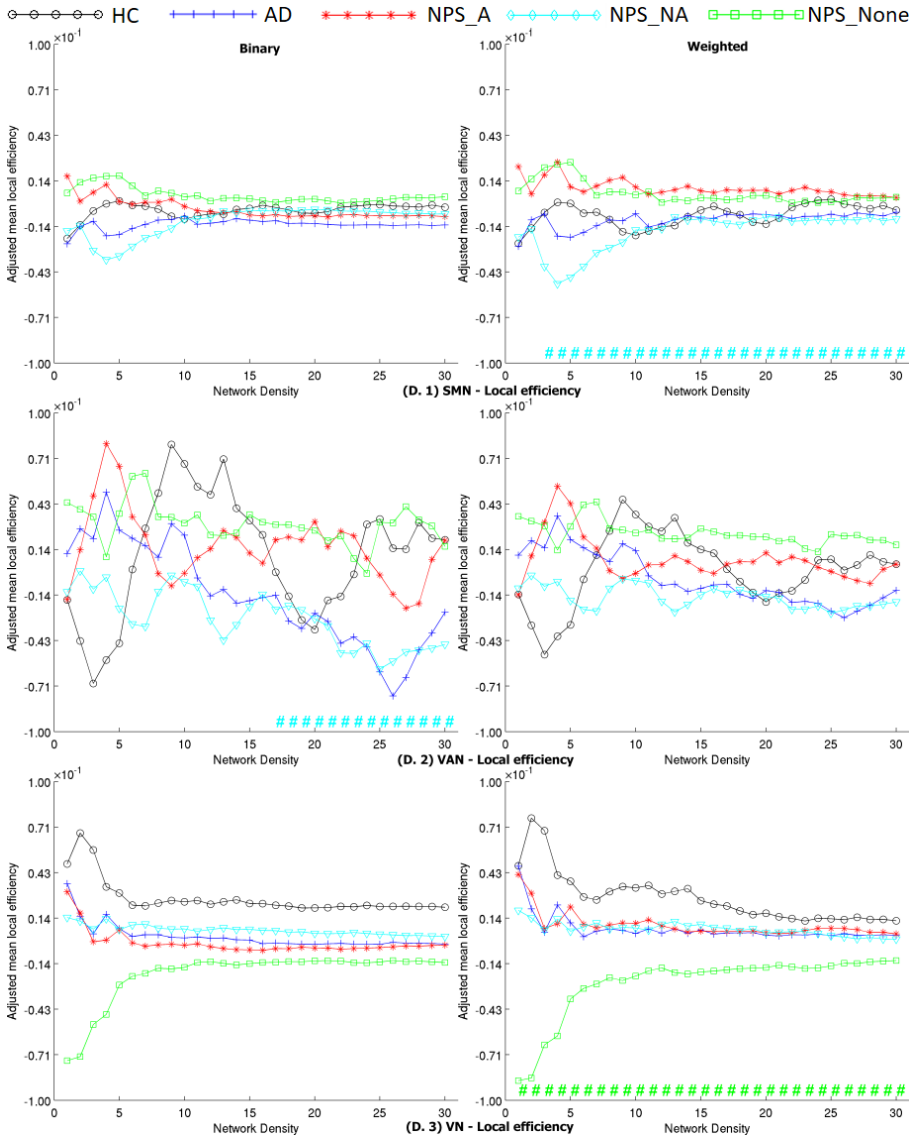
HC
AD
NPS_A
NPS_NA
NPS_None
Binary
Weighted
Adjusted mean local efficiency
Network Density
(D. 1) SMN - Local efficiency
(D. 2) VAN - Local efficiency
(D. 3) VN - Local efficiency

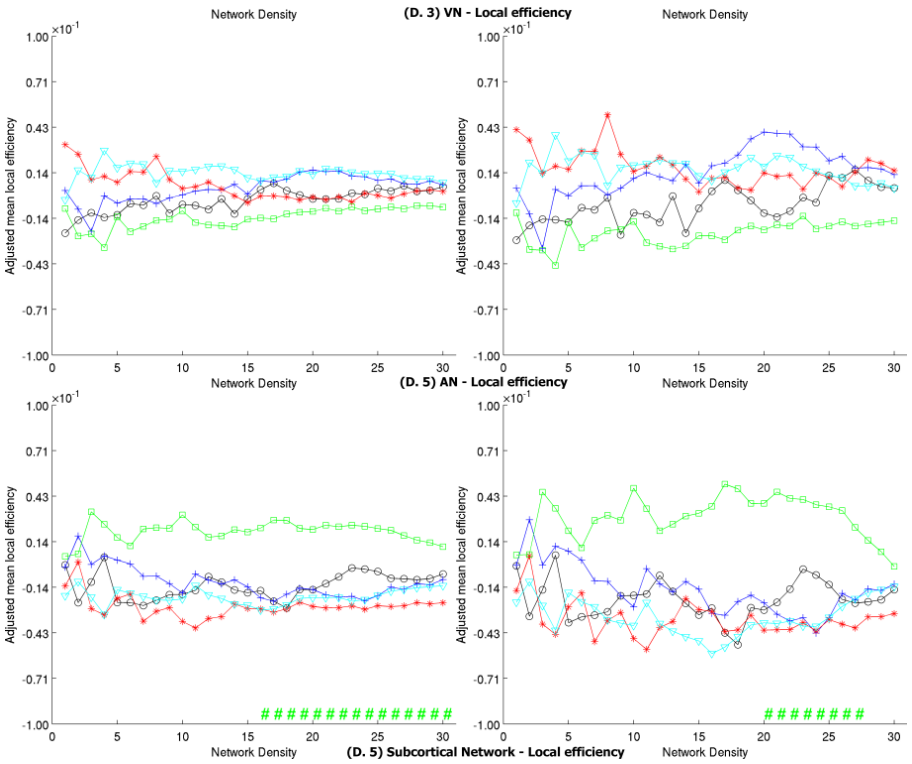
(D. 3) VN - Local efficiency
(D. 5) AN - Local efficiency
(D. 5) Subcortical Network - Local efficiency
Network Density
Adjusted mean local efficiency
×10^-1
1.00
0.71
0.43
0.14
-0.14
-0.43
-0.71
-1.00
0
5
10
15
20
25
30
##############
########

SI Figure E

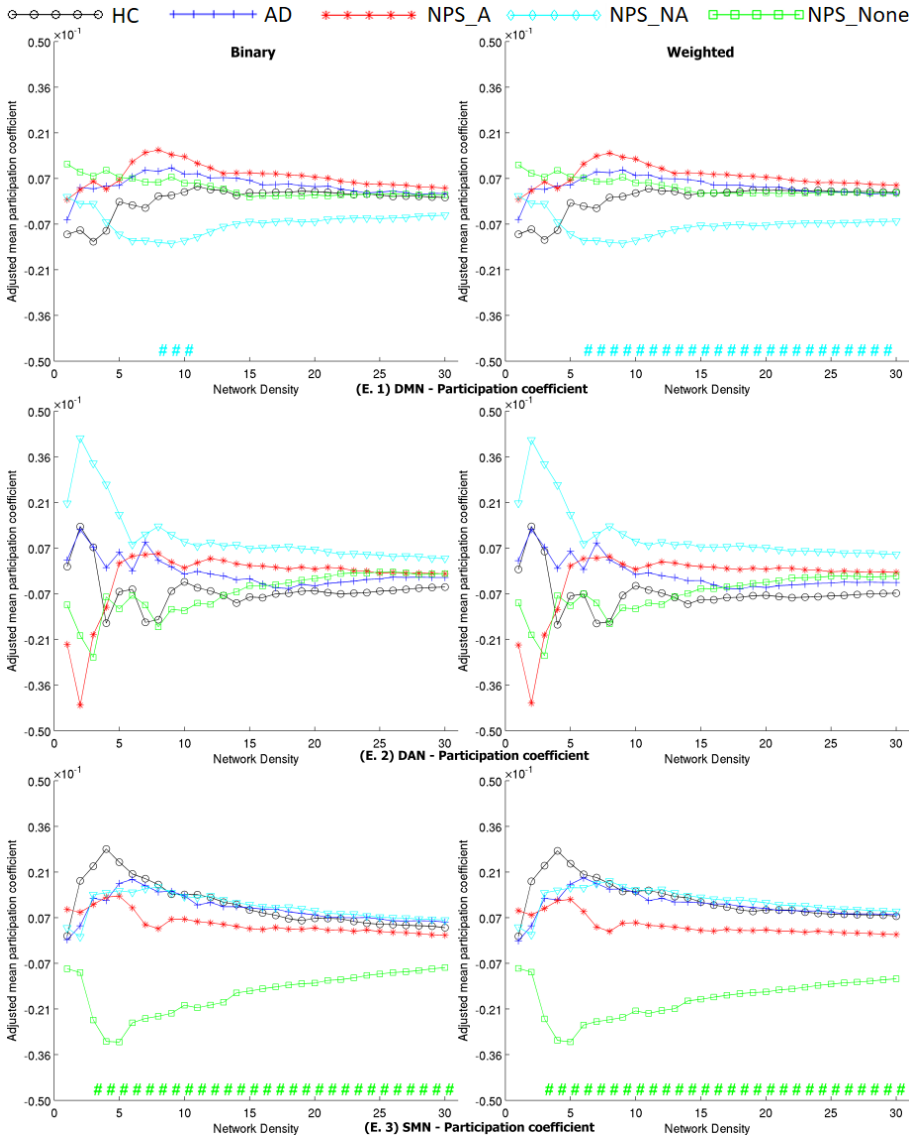
HC
AD
NPS_A
NPS_NA
NPS_None
Binary
Weighted
Adjusted mean participation coefficient
Network Density
(E. 1) DMN - Participation coefficient
(E. 2) DAN - Participation coefficient
(E. 3) SMN - Participation coefficient

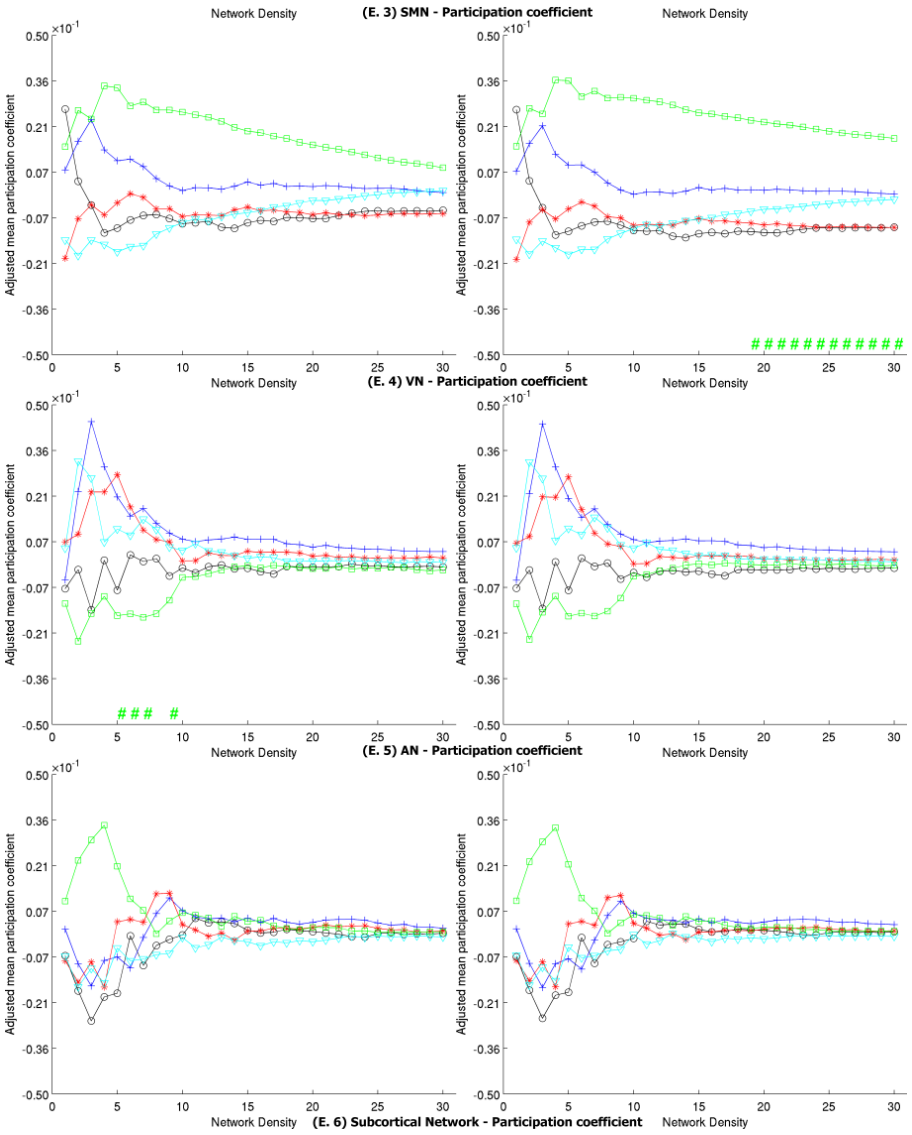
(E. 3) SMN - Participation coefficient
(E. 4) VN - Participation coefficient
(E. 5) AN - Participation coefficient
(E. 6) Subcortical Network - Participation coefficient
Network Density
Adjusted mean participation coefficient
×10-1
0.50
0.36
0.21
0.07
-0.07
-0.21
-0.36
-0.50
0
5
10
15
20
25
30
###########
#